Available online at www.sciencedirect.com
ScienceDirect
Journal of Power Sources 160 (2006) 997–1002
JOURNAL OF POWER SOURCES
www.elsevier.com/locate/jpowsour

Carbon fibers with cup-stacked-type structure: An advantageous support for Pt–Ru catalyst in methanol oxidation

Inês Rabelo de Moraes, Welliton José da Silva, Simone Tronto, Jose Mauricio Rosolen *

Departamento de Química, FFCLRP, Universidade de São Paulo, Av. Bandeirantes, 3900, Ribeirão Preto 14040-901, SP, Brazil

Received 21 December 2005; received in revised form 3 February 2006; accepted 6 February 2006
Available online 22 March 2006

Abstract

Carbon fibers with dangling bonds lined up in an orderly way on the wall of the carbon tube and with an average tube diameter of about 25 nm were studied as support for Pt–Ru nanoparticles. These nanoparticles were prepared using a non-ionic water-in-oil microemulsion (w/o) formed by polyethylenglycol–dodecylether, *n*-heptane, and water. To evaluate the electrochemical performance of this novel catalyst, Pt–Ru nanoparticles supported on carbon Vulcan XC were also prepared by the microemulsion method for comparison. Transmission electron microscopy, X-ray diffraction, energy-dispersive X-ray analysis, and nitrogen adsorption were used to investigate the carbon-supported Pt–Ru catalysts. The microemulsion method furnished Pt_{50}–Ru_{50} particles with average particle sizes of 4.0 ± 0.8 nm, for both carbon supports. The electrocatalytic activity of the supported alloys in methanol oxidation was investigated by cyclic voltammetry and chronoamperometry. Results reveal that the catalytic activity is enhanced by a factor of two when the carbon nanofibers are used as support for the Pt–Ru nanoparticles. The electronic conductivity of the carbon fibers and dangling bonds seem to be the factors responsible for the excellent performance exhibited by the electrodes.

Keywords: Methanol oxidation; Microemulsion; Carbon nanotubes; Catalyst; Pt–Ru nanoparticles

1. Introduction

Fuel cells are an attractive power source for a wide range of applications, including transportation and portable electronic devices [1,2]. For example, a typical direct methanol oxidation fuel cell (DMFC) is generally based on highly dispersed Pt-based nanoparticles either immobilized on an inert carbon support or deposited directly onto proton exchange membranes (PEM). However, this catalyst's activity at temperatures currently considered for fuel cell applications is far from satisfactory. The catalytic activity of Pt-based catalysts may be influenced by many factors, among which the carbon-supported material plays an important role, since it is used as support for the catalysts. Carbon black has been widely used for immobilization of nanosized metallic particles. Although its high surface area generally enhances particle dispersion, the presence of micropores limits its use as catalyst because the metallic particles get trapped in the micropore and become inaccessible, as observed in the case of methanol molecules [3]. In the last years, carbon nanotubes [4–17] have been applied as alternative supports for metal catalysts. It was found that carbon nanotubes (CNTs) can provide catalysts with better electrochemical performance in the fuel cells than those supported on commercial carbon (carbon black–Vulcan XC) [11–17]. The tubular morphology and the high electrical conductivity of CNTs have been claimed to be the main factors responsible for such findings.

In the search for highly active catalyst electrodes, carbon fibers containing high density of dangling bonds lined up on their outer surface have been applied as supports for Pt–Ru catalysts prepared and probed for methanol oxidation. To the best of our knowledge, only few papers have focused on Pt–Ru/CNTs as catalyst for methanol oxidation [18–21]. The carbon nanofibers (fibers) studied herein present zones where it is possible to see carbon nanotubes bearing a cup-stacked structure (CSCNTs); i.e., a stacking morphology of truncated conical graphene, with large amounts of open edges on the outer surface and empty central channels. In these fibers, the dangling bonds are found throughout the surface of the fibers, which is a result of the edges

* Corresponding author. Tel.: +55 16 3602 4838; fax: +55 16 3633 8151.
E-mail address: rosolen@ffclrp.usp.br (J.M. Rosolen).

0378-7753/$ – see front matter © 2006 Elsevier B.V. All rights reserved.
doi:10.1016/j.jpowsour.2006.02.014

of the truncated conical structure. For single-walled (SWNTs) or multi-walled nanotubes (MWNTs), the dangling bonds are expected to be present in smaller amounts, on walls or opened tips, mainly when submitted to purification methods (e.g., treatment with HNO_3). Applications of this new class of carbon fibers have not been extensively studied because they are not as easily prepared as SWNTs or MWNTs. These fibers morphology, diameter, and length are strongly dependent on the preparation method. For example, Endo et al. [22] have proposed a method that provides carbon fibers with cup-stacked structure, but with internal canals of 50–150 nm, while the fibers studied herein have an external diameter of only 25 nm. Results presented in this paper show that the use of this new kind of fiber bearing with a cup-stacked structure combined with the microemulsion method can improve the electrochemical performance of electrodes for DMFCs. This improvement is attributed to the electronic and percolation effects of the electrode prepared with the carbon fibers presented herein.

2. Experimental

The fibers used in this work were produced via chemical decomposition of methanol on Mn, Co catalyst using zeolite substrates. More details about this method will be published elsewhere. Before impregnation with Pt–Ru nanoparticles, the fibers were cleaned in concentrated HCl/HF under reflux, rinsed several times with water, and dried under vacuum at 100 °C. For comparison, carbon Vulcan XC was also used as support for the catalyst, and it was pre-treated in argon atmosphere at 850 °C for 5 h before use.

The platinum–ruthenium nanoparticles were synthesized by the microemulsion technique [23]. The Pt–Ru nanoparticles were prepared by mixing two microemulsions formed by Brij®30 (polyethylenglycol–dodecylether), *n*-heptane, and water in the same composition. One microemulsion contained H_2PtCl_6 and $RuCl_3$ salts solubilized in water, the other contained the precipitating agent ($NaBH_4$). After the formation of Pt–Ru particles in the microemulsion, an appropriate amount of fibers or carbon Vulcan XC support was dispersed in the microemulsion solution by ultrasound for 1 h, and constant stirring for 24 h. The supported catalysts were separated from the microemulsion solution in a centrifuge, washed several times with acetone and ultra-pure water in order to eliminate surfactant molecules, and finally dried at 40 °C. The atomic composition of the Pt–Ru catalysts was determined by energy-dispersive X-ray (EDX) analysis in a scanning electron microscope (DSM 960 Zeiss) equipped with a Link Analytical QX 2000 microanalyzer and a SiLi detector. Measurements were carried out at 20 keV.

Mirror-finished polished glassy carbon disc electrodes (Sigradur G from Hochtemperatur Werkstoffe GmbH, 9 mm diameter) were used as substrates for the thin-film Pt–Ru/fibers electrodes in the electrochemical measurements. The thin-film electrodes were prepared using the method developed by Schmidt et al. [24]. In short, the catalysts were dispersed ultrasonically in water ($2\,mg_{cat}\,mL^{-1}$), and 40 μL aliquots were transferred onto the glassy carbon substrates. After evaporation of the water under an argon stream, an aqueous Nafion solution was pipetted onto the catalyst film, which was then dried in the argon stream to fix the catalyst film to the substrate. The obtained thin-film of Pt–Ru/fibers electrode was used as the working electrode. For comparison, Pt–Ru/Vulcan XC electrodes were also prepared under the same conditions.

The surface areas of the fibers, Vulcan XC, Pt–Ru/fibers and Pt–Ru/Vulcan XC were determined by nitrogen adsorption at liquid nitrogen temperature in a Nova 1200 Quantachrome Corporation instrument. The surface morphology of the supported catalysts was observed by transmission electron microscopy (TEM) at 80 keV, using a Carl Zeiss A CEM 902 microscope coupled to a slow-scan Proscan camera model HSC-2. TEM samples were prepared by placing a droplet of a sonicated catalyst suspension in water on a clean holey copper grid, which was then dried under ambient conditions. The TEM images were analyzed with the software *Analysis*. To determine the mean diameter and size distribution of the nanoparticles, several TEM micrographs were collected for each sample. X-ray diffraction (XRD) patterns of Pt–Ru/Vulcan XC and Pt–Ru/CSCNT catalysts were collected in a URD-6 Carl Zeiss-Jena diffractometer equipped with an area detector, using a Cu Kα source (λ = 1.5406 Å). The XRD diffractograms were obtained at a scan rate of $0.05\,s^{-1}$ for 2θ values between 30 and 100°. The catalysts particle sizes and lattice parameter were evaluated using the peak associated to the (2 2 0) face of the fcc platinum lattice at $2\theta = 67$, at a scan rate of $0.02°\,s^{-1}$.

All electrochemical measurements were taken in a three-electrode cell at 25 °C. Before both the CO stripping and methanol oxidation reaction were studied, the thin-film electrodes were cycled between 0.07 and 0.9 V versus RHE in an oxygen-free solution of 0.5 M H_2SO_4, in order to control the system cleanliness. For the CO stripping, CO was bubbled into the electrochemical cell and the potential was set at 70 mV for 15 min to ensure CO adsorption. This potential was chosen because it is below the threshold potential at which the adsorbed CO would be electro-oxidized to CO_2 [25]. CO dissolved in the electrolyte was removed by degassing the electrolyte with N_2 for 30 min. Finally, two cyclic voltamograms were recorded between 0.07 and 0.9 V versus RHE at a scan rate of $20\,mV\,s^{-1}$. Potentials higher than 0.9 V were avoided in order to prevent ruthenium dissolution [26]. Subsequently, the electrode was transferred to a second cell containing a 2 M CH_3OH + 0.5 M H_2SO_4 solution, and the behavior of the catalysts was studied by cyclic voltammetry and chronoamperometry. The chronoamperometric currents were recorded for 30 min at a potential of 0.5 V.

3. Results and discussion

The different morphologies of the Pt–Ru/Vulcan XC and Pt–Ru/fibers catalysts are shown in the TEM images in Fig. 1. Vulcan XC consists of carbon spheres with a diameter of approximately 40 nm (Fig. 1a), while the fibers (Fig. 1b) are predominantly composed of a stack of truncated conical graphenes bonded by Van der Waal's interactions, with a hollow central channel (Fig. 1c). The carbon fibers have an external diameter

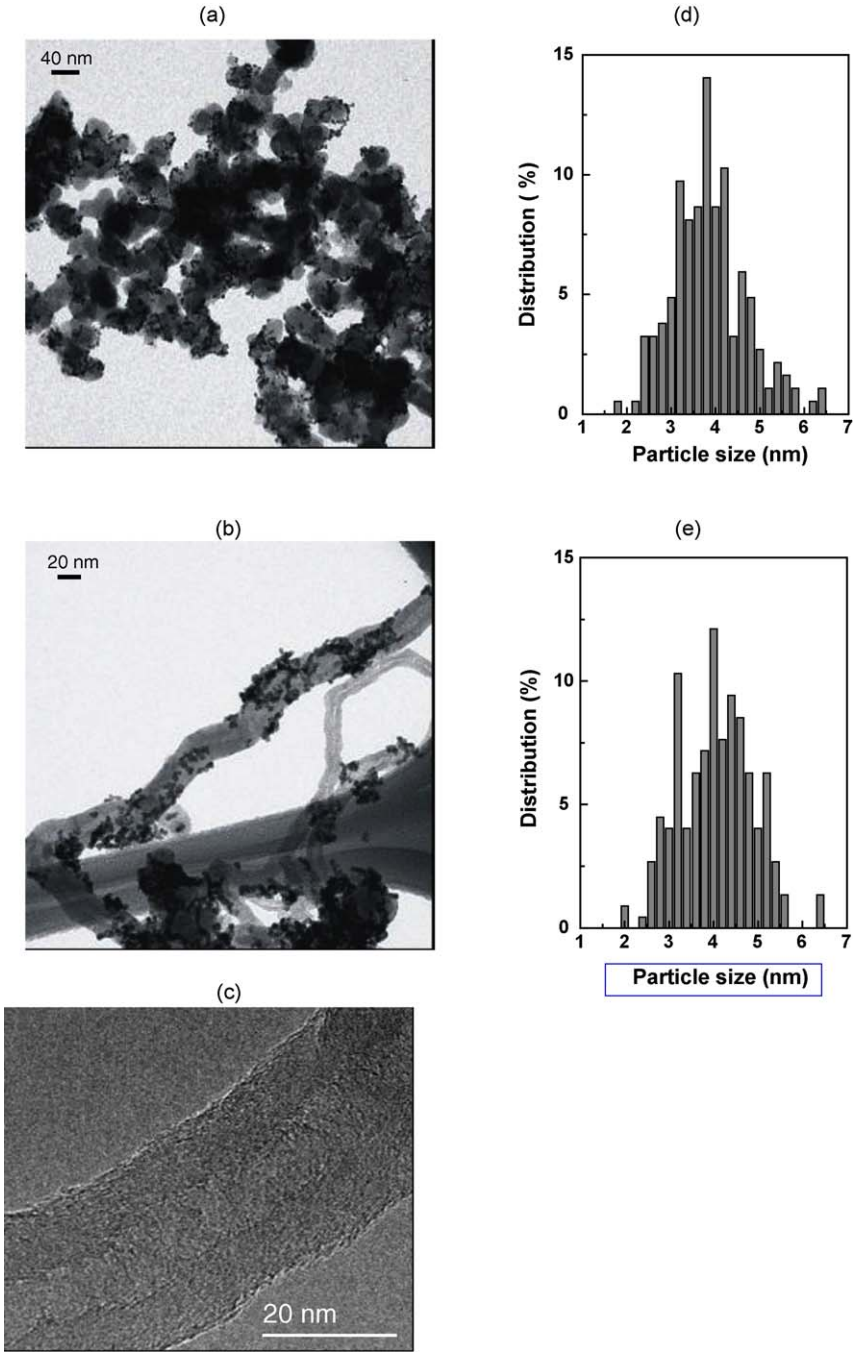

Fig. 1. TEM micrographs of Pt_{50}–Ru_{50}/Vulcan XC (a), and $Pt_{50}Ru_{50}$/fibers (b), detail of the fibers zone containing dangling bonds resulting from large amounts of open edges at the outer surface (c), and their corresponding particle size distributions (d and e).

of 25 nm, and the width of the internal canal is about 13 nm. For both kinds of carbon support, the TEM pictures show that the microemulsion method applied herein provides good dispersion of the Pt–Ru nanoparticles on both carbon supports. Typical histograms for the Pt–Ru/Vulcan XC and Pt–Ru/fibers size distribution are shown in Fig. 1d and e, respectively. Although the particle size distributions observed for the Pt–Ru/Vulcan XC and Pt–Ru/fibers catalysts are slightly different, their average particle sizes are almost the same, 4.2 ± 0.9 nm and 4.0 ± 0.8 nm, respectively. This shows that the microemulsion method used herein provides catalyst dispersion that is similar to that obtained in the case of Pt–Ru/C Vulcan XC, and the particles have virtually the same diameter. Another interesting result observed by means of the TEM analyses is that the density of the particles deposited on the tubes with diameter below 25 nm is very low. Tubes with a diameter of about 15 nm; i.e., MWNTs, have lower particle density than the tubes with a diameter of 25 nm or more. A perfect distinction between carbon fibers and MWNTs is not always evident. Carbon fibers are frequently thicker, typically between hundreds of nanometers to hundreds of microns thick. They present low degree of graphitization and they are frequently found in a structure that is different from that the tubular

Table 1
Surface area determined by BET

Samples	SA ($m^2\ g^{-1}$)
Vulcan XC	216.1
Fibers	146.4
Pt_{50}–Ru_{50}/Vulcan XC	113.4
Pt_{50}–Ru_{50}/fibers	100.5

structure encountered in nanotubes. However, it is well known that when the fiber diameter decreases and the structure becomes more graphitized, the characteristics of the fibers become closer to those of MWNTs. Thus, it is reasonable to suppose that fiber structures rich in dangling bonds provide sites with lower energy than the sites found in the wall of classical MWNTs, where the occurrence of dangling bonds on the tubes' wall is not expected. The carbon Vulcan XC spheres, which allow incorporation of a high number of nanoparticles, have a surface that is also rich in dangling bonds, thus supporting this hypothesis.

The specific surface areas (SSA) of Vulcan XC and of the fibers used as support for Pt–Ru nanoparticles were analyzed before and after the adsorption of the Pt–Ru nanoparticles, by means of the adsorption isotherm. Results are presented in Table 1. The areas for the fibers and Vulcan XC are 113.4 and 216.1 $m^2\ g^{-1}$, respectively. The nitrogen adsorption isotherms of all carbons can be classified as isotherm Type II. According to the IUPAC definitions, this type of isotherm suggests a non-porous or macroporous material. After the anchoring of Pt–Ru nanoparticles, the SSA values decrease to 100.5 $m^2\ g^{-1}$, for the Pt–Ru/fibers, and to 146.4 $m^2\ g^{-1}$, for Pt–Ru/Vulcan XC. The decrease in the SSA with catalyst adsorption is associated with the level of agglomeration of the carbon spheres or dangling bond fibers in the sample. TEM pictures show that in both kinds of carbon support, it is possible to find nanoparticles agglomerates and/or fibers or sphere surfaces where there is no catalyst. Thus, the larger decrease in the SSA observed for Vulcan XC indicates that the nanoparticles are more agglomerated in the Pt–Ru/Vulcan XC powder than in the Pt–Ru/fibers powder, since the isotherms of all the samples belong to Type-II. The composition of the Pt–Ru catalysts was analyzed by EDX, and it indicated a Pt:Ru molar ratio close to 1:1 for both catalysts prepared herein. The nominal and atomic compositions calculated by EDX are almost identical, showing that the microemulsion technique is also an effective way of obtaining catalysts for fuel cells in the desired composition.

To analyze the crystal structure and lattice parameters of the Pt–Ru catalysts the powder X-ray diffraction (XRD) technique was used. The XRD patterns obtained for Pt_{50}–Ru_{50}/fibers and Pt_{50}–Ru_{50}/Vulcan XC catalysts are shown in Fig. 2. Both catalysts show reflections characteristic of the face-centered cubic (fcc) platinum structure. Neither visible peaks associated with tetragonal RuO_2 nor hexagonal close-packed (hcp) Ru phases were observed, which could indicate the alloying of Pt and Ru. The peaks at $2\theta = 40.5$, 46.2, 68.5, and 82.8° can be assigned to the Bragg reflections of the Pt–Ru(1 1 1), Pt–Ru(2 0 0), Pt–Ru(2 2 0), and Pt–Ru(3 1 1) crystallographic planes. The main difference between the two XRD patterns

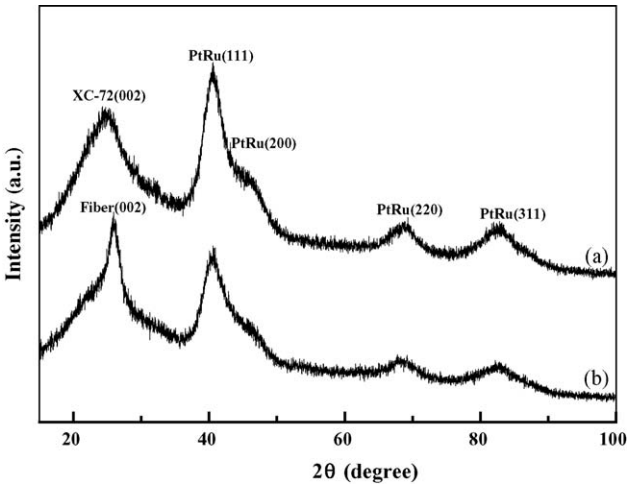

Fig. 2. X-ray diffractograms of Pt_{50}–Ru_{50}/Vulcan XC (a) and $Pt_{50}Ru_{50}$/fibers (b).

shown in Fig. 2 is the peak originated from the carbon support. The broad peak centered at $2\theta = 25°$ in the XRD spectrum can be attributed to the Vulcan XC carbon in the Pt_{50}–Ru_{50}/Vulcan XC catalyst (Fig. 2a), while the sharp peak centered at $2\theta = 26°$ in the XRD spectrum can be attributed to the structure (0 0 2) of the supporting fibers (Fig. 2b). Peak positions in the XRD patterns are not significantly affected by the carbon-support material and they are similar to those obtained in the case of the pure Pt_{50}–Ru_{50} alloy, as determined by Gasteiger et al. [27]. Therefore, the nanoparticles observed in Fig. 1b and c are effectively a Pt–Ru alloy.

Fig. 3 compares the cyclic voltamograms of 20% Pt_{50}–Ru_{50}/Vulcan XC, and 20% Pt_{50}–Ru_{50}/fibers in 0.5 M H_2SO_4 solution, between 0.05 and 0.9 V, at a scan rate of 20 mV s^{-1}. In order to compare the electrochemical results obtained with the different catalysts, all currents (Figs. 3–6) were normalized using the surface area of Pt–Ru bimetallic particles determined by CO_{ads}-stripping voltammetry, assuming that there is formation of a monolayer of linearly adsorbed CO and that the Coulombic charge required for oxidation of CO_{ads} is

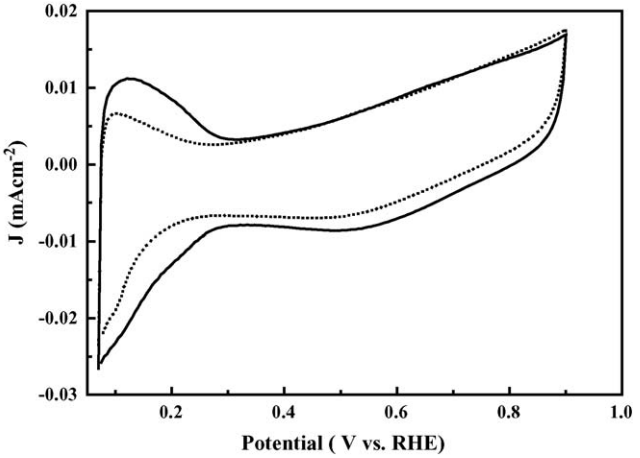

Fig. 3. Cyclic voltamograms of Pt_{50}–Ru_{50}/Vulcan XC (···), and Pt_{50}–Ru_{50}/fibers (—) in 0.5 M H_2SO_4, at a scan rate of 20 mV s^{-1}.

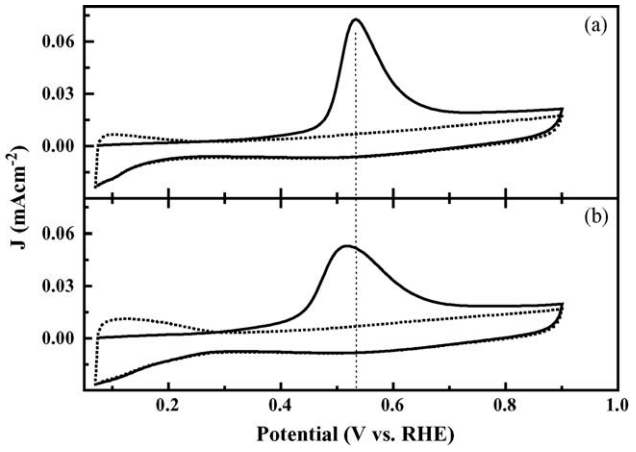

Fig. 4. CO stripping voltammograms on Pt_{50}–Ru_{50}/Vulcan XC (a), Pt_{50}–Ru_{50}/fibers in 0.5 M H_2SO_4 (b), at a scan rate of 20 mV s^{-1}.

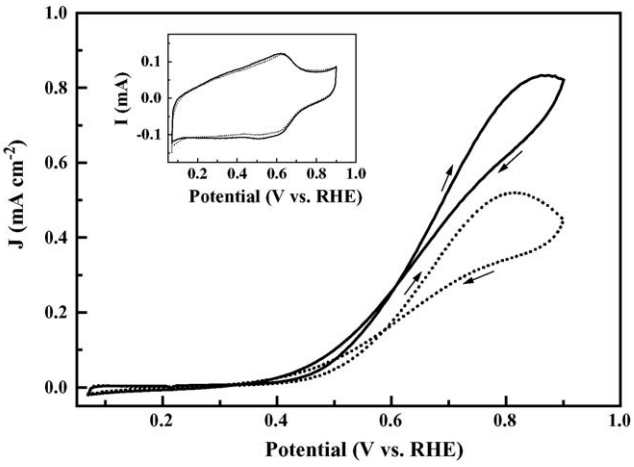

Fig. 5. Methanol oxidation on (···) Pt_{50}–Ru_{50}/Vulcan XC, and (—) Pt_{50}–Ru_{50}/fibers in 0.5 M H_2SO_4 + 2 M CH_3OH, at a scan rate of 20 mV s^{-1}. The inset shows the cyclic voltammograms of the fibers before the Pt–Ru particles deposition in 0.5 M H_2SO_4 (···) and 0.5 M H_2SO_4 + 2 M CH_3OH (—) electrolytes.

420 μC cm^{-2}. For the Pt–Ru/C Vulcan XC catalyst, the hydrogen adsorption/desorption region (0.07–0.35 V) is less resolved than in the case of Pt–Ru/fibers. The hydrogen adsorption charge is enhanced by almost six times when fibers are used as support for the Pt–Ru nanoparticles, accounting for its higher catalytic activity and the possible insertion of H_2 inside the fibers, since the walls are open. The double layer region of Pt_{50}–Ru_{50}/fibers is also slightly larger than that of Pt_{50}–Ru_{50}/Vulcan XC.

Fig. 4 shows the CO_{ads}-stripping voltammograms of Pt_{50}–Ru_{50}/Vulcan XC and Pt_{50}–Ru_{50}/fibers catalysts in 0.5 M H_2SO_4. The absence of peaks in the hydrogen region of the first sweep clearly indicates that the surface of these two catalysts was saturated with CO. The voltamograms show that the shape and position of the CO oxidation peak are slightly dependent on the substrate used as support for the nanoparticles. For the Pt_{50}–Ru_{50}/Vulcan XC catalyst (SSA = 113.4 m^2 g^{-1}), the onset of the CO stripping peak takes place at about 0.37 V, and a sharp peak is formed at 0.53 V versus RHE. In the case of Pt_{50}–Ru_{50}/fibers (SSA = 100.5 m^2 g^{-1}), the onset of CO oxidation takes place at 0.31 V, and a broader peak centered at 0.51 V is observed. Carmo et al. [19] also found a broad peak centered at 0.55 V versus RHE for CO oxidation on Pt–Ru/MWNT prepared by the impregnation method. However, no influence of the carbon support on the CO oxidation peak position could be seen.

The electrocatalytical activity of the Pt_{50}–Ru_{50}/fibers before and after Pt–Ru deposition was investigated by cyclic voltammetry in 2 M CH_3OH + 0.5 M H_2SO_4 solution, and the results were compared with those obtained by using the Pt_{50}–Ru_{50}/Vulcan XC catalyst. As can be seen in the inset of Fig. 5, the shapes of cyclic voltammograms collected from the carbon fibers in 0.5 M H_2SO_4 and 2 M CH_3OH + 0.5 M H_2SO_4 solutions, and in 0.5 M H_2SO_4 are identical; only background currents typical of carbon electrodes are seen. This means that the carbon fibers do not display electrocatalytical activity for methanol oxidation. After Pt–Ru deposition on the fibers, higher currents of methanol oxidation can be observed. A comparison of the anodic currents for methanol oxidation on the Pt_{50}–Ru_{50}/fibers and Pt_{50}–Ru_{50}/Vulcan XC catalysts shows that the onset of methanol oxidation begins at ca. 0.4 V versus RHE for both electrodes. For potentials more positive than 0.4 V, higher methanol oxidation currents can be found for Pt_{50}–Ru_{50}/fibers. In the cathodic scan, the re-oxidation of methanol is clearly observed due to the reduction of platinum oxide.

To test the tolerance of the Pt–Ru catalysts to methanol oxidation, we collected chronoamperometric curves at 0.5 V versus RHE in a 2.0 M CH_3OH + 0.5 M H_2SO_4 solution. As can be seen in Fig. 6, the potentiostatic currents decrease rapidly at short reaction times. At long times and for all potentials, the rate of current decay is small and a pseudo-steady state current is achieved. The current densities recorded after holding the electrode potential at 0.5 V for 1800 s were 0.041 mA cm^{-2} for Pt_{50}–Ru_{50}/fibers, and 0.025 mA cm^{-2} for Pt_{50}–Ru_{50}/Vulcan XC. This shows that the current density for the $Pt_{50}Ru_{50}$/fibers catalyst is 1.6 times higher than that observed with the Pt_{50}–Ru_{50}/Vulcan XC catalyst.

All these findings thus suggest that the fibers with CSCNTs zones, together with the microemulsion method, allow the prepa-

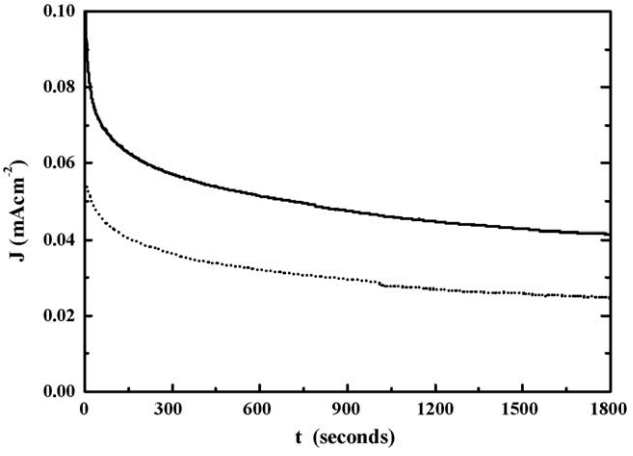

Fig. 6. Chronoamperometries for 30 min at 0.5 V vs. RHE for Pt_{50}–Ru_{50}/Vulcan XC (···), and Pt_{50}–Ru_{50}/fibers (—) in 0.5 M H_2SO_4 + 2 M CH_3OH.

ration of catalysts with enhanced catalytic activity for methanol oxidation. The dangling bond in these fibers allows similar dispersion to that found in the case of Vulcan XC, when the microemulsion method is applied. However, the agglomeration of the fibers with high density of dangling bonds is smaller in the fibers than in Vulcan carbon, as detected by BET characterization. This means that the methanol percolation is better in the Pt_{50}–Ru_{50}/fibers electrode than in the Pt_{50}–Ru_{50}/Vulcan XC. The morphology of the fibers studied herein favors a less hydrophobic surface than that encountered in MWNTs or SWNTs. In fact, we checked this by comparing the dispersion of cup-stacked fibers with MWNTs or SWNTs, both in water and methanol. Simulation studies demonstrated that methanol and water enter the pores of hydrophilic nanotubes more easily [28]. Therefore, fluid transport through the hydrophilic tubes is faster than through hydrophobic carbon nanotubes. This means it is reasonable to believe that the catalyst supported on the fibers (Fig. 1b) has a higher electrochemical active surface area than that prepared with Vulcan XC. The electrochemical area determinate by CO stripping was 9.4 cm^2 for the Pt_{50}–Ru_{50}/Vulcan XC and 19.4 cm^2 for Pt_{50}–Ru_{50}/fiber.

The catalyst prepared with fibers (Fig. 1b) has, thus, a higher electrochemical active surface area than the catalyst prepared with Vulcan XC. Finally, another factor that can be related to the enhancement in methanol oxidation by using the Pt_{50}–Ru_{50}/fibers catalyst is the high electronic conductivity of the nanotubes used as support. Atomic Force Microscopy (AFM) with conductivity set-up shows for us that the carbon fibers studied herein are metallic, like the multi-walled carbon nanotubes. As already known, carbon nanotubes exhibit high electronic conductivity, and therefore, all the catalysts that are connected to them are also connected to the conductivity and can thus be used. In addition, emission results suggest that the graphene planes can act as electron channels [29].

4. Conclusions

In this work, carbon nanotube fibers with high density of dangling bonds and carbon Vulcan XC were used as support for Pt–Ru nanoparticles prepared by the microemulsion method. The microemulsion method was found to be a convenient way of obtaining small and homogeneous particles with different compositions, without being influenced by the morphology of the fibers studied herein. Our results showed that the Pt–Ru/fibers electrode exhibits higher catalytic activity than Pt–Ru/Vulcan XC for methanol oxidation. The higher catalytic activity obtained by using this new kind of fibers as support for Pt–Ru nanoparticles can be attributed to the morphology of the unique nanostructure and electronic properties of the carbon tubes.

Acknowledgements

The authors thank Fundação de Amparo à Pesquisa do Estado de São Paulo (FAPESP: 00/15080-0, 03/11818-2 and 04/07085-2), and CNPq for financial support. Instituto do Milênio/IQ-UNICAMP and LNLS for the use of TEM. We also thank L.A. Montoro for technical support in the obtention of the HRTEM pictures.

References

[1] S.R. Narayanan, T.I. Valdez, in: V. Wolf, L. Arnold, A. Hubert, Gasteiger (Eds.), Handbook of Fuel Cells, Fundamental, Technology and Application, 4th ed., John Wiley & Sons, 2003, p. 1133.
[2] S. Wasmus, A. Küver, J. Electroanal. Chem. 461 (1999) 14–31.
[3] H. Shi, Electrochim. Acta 41 (1996) 1633–1639.
[4] R. Yu, L. Chen, Q. Liu, J. Lin, K.L. Tan, S.C. Ng, H.S.O. Chan, G.Q. Xu, T.S.A. Hor, Chem. Mater. 10 (1998) 718–722.
[5] H.C. Choi, M. Shim, S. Bandsaruntip, H. Dai, J. Am. Chem. Soc. 24 (2002) 9058–9059.
[6] D.J. Guo, H.L. Li, J. Electroanal. Chem. 573 (2004) 197–202.
[7] C.L. Sun, L.C. Chen, M.C. Su, L.S. Hong, O. Chyan, C.Y. Hsu, K.H. Chen, T.F. Chang, L. Chang, Chem. Mater. 17 (2005) 3749–3753.
[8] H. Tang, J. Chen, S. Yao, L. Nie, Y. Kuang, Z. Huang, D. Wang, Z. Ren, Mater. Chem. Phys. 92 (2005) 548–553.
[9] C.L. Lee, Y.C. Ju, P.T. Chou, Y.C. Huang, L.C. Kuo, J.C. Oung, Electrochem. Commun. 7 (2005) 453–458.
[10] C.C. Chen, C.F. Chen, C.H. Hsu, I.H. Li, Diamond Relat. Mater. 14 (2005) 770–773.
[11] Y. Lin, X. Cui, C. Yen, C.M. Wai, J. Phys. Chem. B 109 (2005) 14410–14415.
[12] J.E. Huang, D.J. Guo, Y.G. Yao, H.L. Li, J. Electroanal. Chem. 577 (2005) 93–97.
[13] G. Wu, Y.S. Chen, B.Q. Xu, Electrochem. Commun. 7 (2005) 1237–1243.
[14] T. Matsumoto, T. Komatsu, K. Arai, T. Yamazaki, M. Kijima, H. Shimizu, Y. Takasawa, J. Nakamura, Chem. Commun. (2004) 840–841.
[15] Y. Xing, J. Phys. Chem. B 108 (2004) 19255–19259.
[16] W. Chen, J. Zhao, J. Yang Lee, Z. Liu, Mater. Chem. Phys. 91 (2005) 124–129.
[17] T. Maiyalagan, B. Viswanathan, U.V. Varadaraju, Electrochem. Commun. 7 (2005) 905–912.
[18] E.S. Steigerwalt, G.A. Deluga, D.E. Cliffel, C.M. Lukehart, J. Phys. Chem. B 105 (2001) 8097–8101.
[19] M. Carmo, V.A. Paganin, J.M. Rosolen, E.R. Gonzalez, J. Power Sources 142 (2004) 169–176.
[20] Y.L. Yao, Y. Ding, L.S. Ye, X.H. Xia, Carbon 44 (2006) 61–66.
[21] Z. He, J. Chen, D. Liu, H. Zhou, Y. Kuang, Diamond Relat. Mater. 13 (2004) 1764–1770.
[22] M. Endo, Y.A. Kim, T. Hayashi, Y. Fukai, K. Oshida, M. Terrones, T. Yanagisawa, S. Higaki, M.S. Dresselhaus, Appl. Phys. Lett. 80 (2002) 1267–1269.
[23] S. Eriksson, U. Nylén, S. Rojas, M. Boutonnet, Appl. Catal. A 265 (2004) 207–219.
[24] T.J. Shimidt, M. Noeske, H.A. Gasteiger, R.J. Behm, J. Electrochem. Soc. 145 (1998) 925–931.
[25] F. Colmati Jr., W.H. Lizcano-Valbuena, G.A. Camara, E.A. Ticianelli, E.R. Gonzalez, J. Braz. Chem. Soc. 13 (2002) 474–482.
[26] B. Beden, F. Kardigan, C. Lamy, J.M. Leger, J. Electroanal. Chem. 127 (1981) 75–85.
[27] H.A. Gasteiger, N. Markovic, P.N. Ross, E.J. Carins, J. Phys. Chem. 97 (1993) 12020–12029.
[28] J. Zheng, E.M. Lennon, H.K. Tsao, Y.J. Sheng, S. Jiang, J. Chem. Phys. 122 (2005) 214702–214708.
[29] X. Ma, E. Wang, W. Zhou, D.A. Jefferson, J. Chen, S. Deng, N. Xu, J. Yuan, Appl. Phys. Lett. 75 (1999) 3105–3107.